Silicon (2023) 15:4943–4957
https://doi.org/10.1007/s12633-023-02406-6

ORIGINAL PAPER

Synthesis of ZnO-Containing Calcium Silicate Nano Powders: A study on Sinterability, Mechanical and Electrical Properties

Rasha A. Youness[1] · Mahmoud F. Zawrah[2] · Mohammed A. Taha[3]

Received: 20 January 2023 / Accepted: 9 March 2023 / Published online: 18 March 2023

Abstract
In this study, amorphous ZnO-containing calcium silicate nano powders were prepared by sol–gel technique and then calcined at different temperatures; namely, 600, 800 and 1000 °C, to study their crystallization. The synthesized powders were examined by X-ray diffraction (XRD) technique, Fourier transform infrared spectroscopy (FTIR) and transmission electron microscopy (TEM). Then, the synthesized powders were sintered at different temperatures. The sintered ceramics were examined for their physical properties, microstructure, mechanical properties and electrical properties by the suitable techniques. The results revealed that the synthesized nano powders were amorphous even after calcination up to 800 °C. By increasing the calcination temperature into 1000 °C, crystalline calcium silicate ceramic was formed. The average particle size of this crystalline material was 50 nm with lower agglomeration among the others calcined at low temperatures. Regarding to the sintered ceramics, the bulk density, fracture toughness and electrical conductivity were increased with increasing both sintering temperature and zinc content. On the other hand, microhardness, compressive strength, elastic moduli and Poisson's ratio were increased with increasing sintering temperature and decreased with increasing the zinc content.

Keywords Calcium silicate · Sol–gel · Mechanical Properties · Electrical properties · ZnO

1 Introduction

Calcium silicates are a class of ceramics which include calcium, silicon and oxygen with various proportions. These elements form many phases and compounds that can be applied as cementitious materials, biomedical, refractory and nuclear applications [4, 21, 22, 53, 59]. For this class of materials, the molar ratio of calcium/silicon is always ranged between 0.5–3.0 [43]. The wet chemical synthesis of these materials might give amorphous powder which gives crystalline phases when fired at high temperature. One of the most interesting systems of these materials is CaO-ZnO-SiO_2 system which has not been intensively studied in the literatures. The following stoichiometric compounds can be formed under the effect of temperature and according to percentage of these oxides, namely, tridymite and cristobalite SiO_2, pseudo wollastonite and wollastonite $CaSiO_3$, rankinite $Ca_3Si_2O_7$, willemite Zn_2SiO_4, and melilite (hardystonite) $Ca_2ZnSi_2O_7$. Also, some solid solution phases as dicalcium-silicate $(Ca,Zn)_2SiO_4$, tricalcium-silicate $(Ca,Zn)_3SiO_5$, lime (Ca,Zn)O, and zincite (Zn,Ca)O can be formed in addition to Ca–Zn feldspar $CaZnSi_3O_8$ and petedunnite (pyroxene) $CaZnSi_2O_6$ phases [19].

It has been recognized that the credit for manufacturing of silicate bioglass goes back to Hench on 1971 [24], who discovered these important species to be utilized in many biomedical applications. Since then, the field has expanded thanks to extensive work by scientists around the world examining different types of bioceramics and bioglasses for the needs of clinical community [3, 46]. Consequently, several researchers have discovered silicate-containing ceramics or glasses based on their potential for use in hard/soft tissue repair. This recommendation is strongly related to their astonishing properties such as appropriate mechanical properties, excellent biocompatibility as well as great ability to promote the cellular attachment and osteoblasts proliferation

✉ Mahmoud F. Zawrah
mzawrah@hotmail.com

[1] Spectroscopy Department, National Research Centre, El Buhouth St., Dokki, Giza 12622, Egypt

[2] Refractories, Ceramics and Building Materials Department, National Research Centre, El Buhouth St., Dokki, Giza 12622, Egypt

[3] Solid State Physics Department, National Research Centre, El Buhouth St., Dokki, Giza 12622, Egypt

[37, 55]. However, caution must be taken when preparing silicate materials in the conventional manner where they lose their ability to bind with living tissues when silica content raises to higher than 55 mol% [52]. Thus, one way to overcome this difficulty is to prepare silicate materials with the help of sol–gel technology or other methods for synthesis of nano materials considering that these methods offer the preparation of desired silicates not only in high purity but also in different forms such as powders and thin films without the need for high temperature [11, 12, 44]. In comparison with the materials prepared by conventional methods, the sol–gel technique gives better bioactivity behavior to prepared materials [1, 5, 29].

It is well common that obtaining optimal biomaterials for orthopedic applications has not been reached yet owing to the massive physical, chemical, biological properties required for such purpose. For example, obtaining biomaterials with outstanding electrical properties has attracted the interest of specialists in this field with the goal of achieving better stimulation of bone growth, induction of osseointegration and increased bone density [8]. Furthermore, the excellent antibacterial effect of human bone implants is highly recommended due to the possible infection arising from surgical operations. In addition, suitable mechanical and tribological properties are in a high demand. For this purpose, metal oxides (MO) can be added to the prepared materials to contribute in improving of the aforementioned properties [9, 10, 34].

Zinc oxide (ZnO) is classified as a semiconductor material with characteristic that falls between ionic and covalent semiconductors. It has been applied for various applications such as electronics, optoelectronics, and laser technology because of its broad energy band, high bond energy, and strong thermal and mechanical stability at ambient temperature. Because of its piezoelectric and pyroelectric capabilities, ZnO may be employed as a hydrogen sensor, converter, energy producer and photocatalyst. It is used in ceramics sector owing to its hardness, stiffness, and piezoelectric constant, while it is also applied in biomedicine and pro-ecological systems due to its low toxicity, biocompatibility, biodegradability and its antibacterial activity [31]. It should be noted that Zn is a prevalent element in both human and natural settings, and it is involved in a wide range of biological activities. Zn as an important trace element or micronutrient is required for optimal development and reproduction in all higher plants, animals and humans. It also performs an immunological function and plays a critical role during physiological development. It is required for the action of over 300 enzymes, the stability of DNA, and the expression of genes [20]. In keeping with the above-mentioned amazing properties, it also shows excellent antibacterial effect which makes it one of the good choices for biomedical applications [26].

The main purpose of this research is to prepare amorphous/crystalline nano CaO-SiO_2-ZnO materials with varying the concentration of ZnO between 2 and 5 mol.%, using the sol–gel process to be applied for different applications. Powder characterization and sintering at different temperatures are also considered in this study. The sintered ceramics are subjected for investigation of physical properties, microstructure, surface roughness, mechanical properties and dielectric characteristics.

2 Materials and Experimental Methods

2.1 Materials

Zinc chloride (98%), tetraethyl orthosilicate (TEOS 99%), calcium nitrate tetrahydrate ($Ca(NO_3)_2{\cdot}4H_2O$, 98%), hexacetyltrimethylammonium bromide (CTAB 98%), absolute ethyl alcohol (C_2H_5OH) and ammonia solution (NH_4OH) were supplied from Sigma-Aldrich.

2.2 Experimental Methods

2.2.1 *Synthesis of CaO-ZnO-SiO_2 Powders by Sol–Gel*

Two calcium silicate samples doped with ZnO were synthesized by sol–gel technique. The mole percentages of these samples were Zn:Ca:Si = 2:13:85 and 5:10:85 (i.e. $Ca_{(15-x)}$-Si_{85}-Zn_x (x = 2 and 5)) as illustrated in Table 1. Firstly, CTAB was dissolved with the help of appropriate amounts of C_2H_5OH and NH_4OH with keeping the pH = 12.5. Then after, $Ca(NO_3)_2{\cdot}4H_2O$ and $ZnCl_2$ were dissolved in that solution. Apart from this solution, TEOS was liquefied alone in C_2H_5OH and mixed with the former prepared solution under mechanical stirring for 20 min. This prepared liquid was subjected for stirring 24 h by mechanical stirring until the reaction is completed. The prepared concentrated suspension was undergone for washing for many times then centrifuged at 3000 rpm for 10 min. and finally dried at 100 °C for 24 h. The synthesized powder was calcined at various firing temperatures, e.g. 600°, 800° and 1000 °C for 2 h at 5 °C/min.

2.2.2 Investigation of Prepared Powders

The qualitative phase-composition of synthesized ceramic powders fired at 600°, 800° and 1000 °C were examined by X-ray deffractometer model "Philips PW 1373″ with Ni filter, Copper Kα-radiation with scan speed of 0.5 min^{-1}. The function groups of synthesized ceramics were predicted by Fourier transform infrared (FTIR) tool, model Jasco 300E Japan, at 25 °C utilizing KBr disc-method in the wave number ranged between 4000 and 400 cm^{-1} under 32-scans at

2 cm^{-1} resolution. The morphological features and particle-sizes of synthesized powder fired at 600°, 800° and 1000 °C were inspected by transmission electron microscope attached by selected area electron-diffraction (TEM-SAED), model JEOL-JEM 2100 Japan, worked at accelerating-voltage of 120 kV.

2.2.3 Sinterability of Synthesized Powders

The CaO-ZnO-SiO_2 powders calcined at 1000 °C were pressed at 50 MPa in cylindrical stainless steel mold having dimensions 16 mm length and 4 mm diameter. The compacted specimens were subjected for sintering process at different temperatures; namely 1000°, 1100°, 1200° and 1300 °C for 2 h in surrounding atmosphere and heat-rate 5 °C/min**.**

2.2.4 *Investigation of Sintered CaO-ZnO-SiO_2*

The bulk density and apparent porosity of sintered specimens were measured giving the Archimedes' principle described elsewhere [40, 49], according to ASTM C20. Three specimens were used for each test and the average value was recorded. The microstructure of specimens sintered at 1100° and 1300 °C was investigated by scanning electron microscope (SEM) model "Philips XL3000". The roughness of sintered samples was evaluated utilizing Gwyddion software version 3.32, to change the two-dimension (2D) FE-SEM images into three-dimension (3D) micrographs. On the other hand, microhardness and fracture toughness as well as compressive strength of sintered silicates were determined giving the ASTM-B933-09 and ASTM-E9, respectively [54, 56]. The ultrasonic longitudinal- (V^2_L) or shear-wave-velocity (V^2_S) transmitted through the specimens has been recorded at 25 °C by Pulse-echo technique MATEC-Model-MBS8000-DSP with 5 MHz resonating. The Lame's parameters (λ and μ) were calculated from V^2_L and V^2_S as described elsewhere [16, 55]. The alternating current electrical-conductivity, dielectric-constant and dielectric-loss of sintered specimens were determined at 25 °C by broadband dielectric system.

3 Results and Discussion

3.1 Characteristics of Synthesized Nano Powders

The effect of calcination temperature on phase composition of prepared nano CaO-SiO_2-ZnO powders as investigated by XRD technique is shown in Fig. 1. From this figure, it is indicated that both calcium silicate materials calcined at 600 and 800 °C have almost amorphous glassy structures since no intense peaks of crystalline phases that arise from

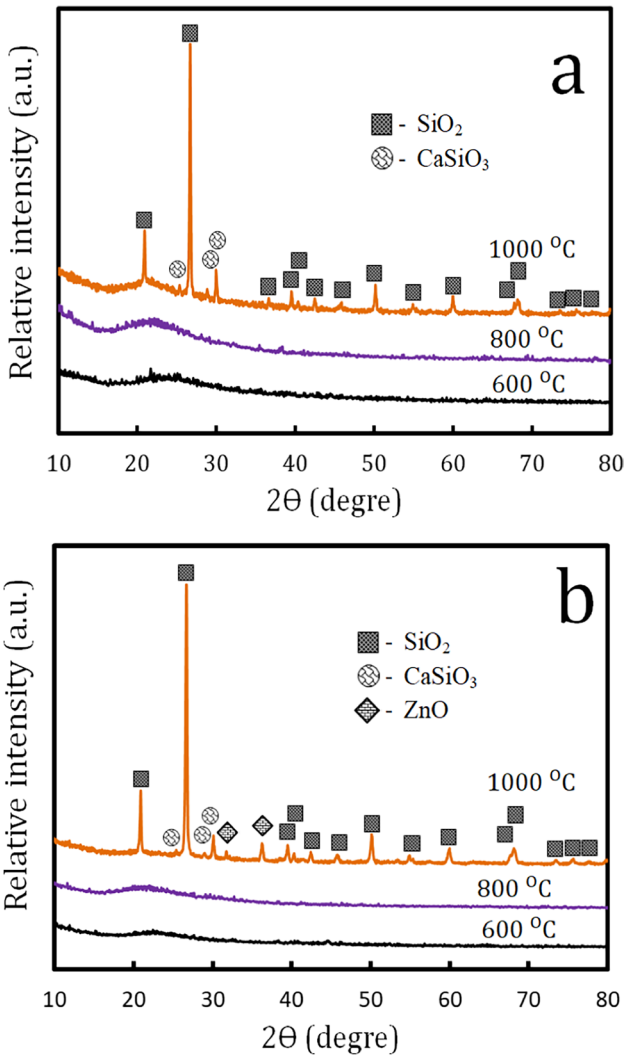

Fig. 1 XRD patterns of a) Zn2 and b) Zn5 samples fired at 600, 800 and 1000 °C

the lattice periodicity, are appeared in the patterns. Only very small broad peak at 2θ equal 20–30° related to amorphous silica is detected with the presence of few small peaks related to incomplete calcined hydrate silicate phases (at 600 °C) or premature crystalline silicate phases (at 800 °C). In contrast, after elevating the calcination temperature into 1000 °C, the aforementioned feature (amorphousity) is disappeared with formation new diffraction peaks reflecting the complete transformation of amorphous glassy structures into crystalline ones; namely into SiO_2, calcium silicate (CS; $CaSiO_3$) and ZnO. The patterns indicate that the main crystalline phase at this temperature is silica with the existence of formed CS; the amount of this phase might increase after increasing the firing temperature. The appearance of ZnO is not confirmed in the sample that contains 2% ZnO since it is below the detection limit of XRD technique. It is worth to mention that the crystalline phases of SiO_2, $CaSiO_3$ and

ZnO are identified according to (intensified charge coupled devices) ICCDs 86–1629, 84–0655 and **89–5899**, respectively. This means that the prepared materials are composed of silica matrix around crystalline calcium silicate and the calcination at the proposed temperatures leads to stabilization the matrix [32]. This material can be applied as filler in injectable replacements which can release silicate, Ca and Zn ions then induce bioactivity and antibacterial activity. It is important to emphasize that the obtained findings are well supported by those discussed in Refs. [7, 32].

It is well known that FT-IR spectroscopy provides accurate analysis of a building's structure and the bonding configuration of materials. In this regard, FTIR spectra of prepared powders fired at various temperatures are shown in Fig. 2. The recorded FT-IR absorption bands are investigated with the help of articles published elsewhere [2, 6, 28, 30, 41, 50]. It is worth mentioning that the increase of zinc content and calcination temperature has a significant effect on the structure and on the formed function groups of bioactive silicates

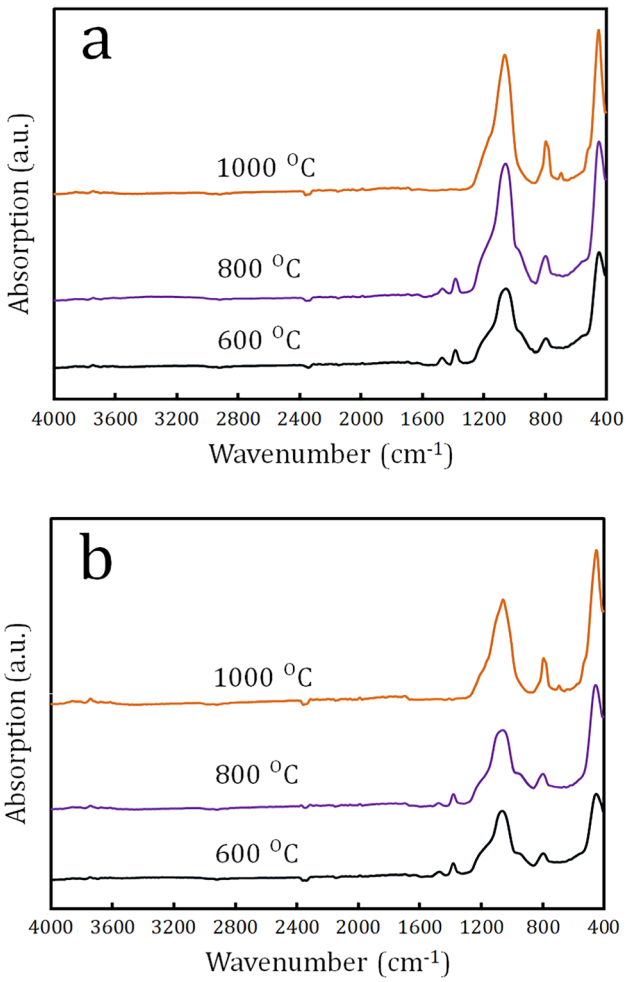

Fig. 2 FTIR absorption spectra of a) Zn2 and b) Zn5 samples fired at 600, 800 and 1000 °C

containing-materials. These silicates open-networks are composed mainly of -SiO_4 tetrahedrons and can accumulate alkali or alkaline earth positive ions which are considered as network modifiers and cause breaking of the network due to break down of Si–O-Si links with the formation of none bridging oxygen groups (Si–O-NBO) [41]. This situation considerably differs in case of Zn since it can enter the silicate network partly (creating Si–O-Zn links) i.e. partly replacing SiO_4 by ZnO_4. The other part can behave as network modifiers for enhancement of the chemical stability with the formation of none bridging oxygen groups (Si–O-NBO) [58]. The existence of calcium and zinc in silicate materials lead to enhancing the chemical stability which slowdown the silicate degradation rate.

As seen in FTIR spectra of calcium silicates calcined at 600 °C, the weak band near 1450 cm^{-1} is attributed to C-O bending vibration of CO_3^{2-} anion that might be produced as a consequence of carbonation process for calcium silicate from surrounding atmosphere as a result of relatively high calcium content in the prepared materials. At 800 °C, this band decreases while it is completely vanished after calcination at 1000 °C due to de-carbonation of materials. For the samples calcined at 600 and 800 °C, tiny band at 1380 cm^{-1} is appeared in the spectra. This band is attributed to anti-symmetric stretching vibration of NO_3^- anion that comes through the remaining traces of nitrate reactants. Due to the evaporation of NO_2 gas during calcination at 1000 °C, this band practically vanishes indicating that fired materials have no free nitrate. The small band at 1200 cm^{-1} is ascribed to symmetric stretching vibration of Si–O–Si bond, whereas bands at 800 and 450 cm^{-1} are attributed to bending vibrations of Si–O and Si–O–Si bonds, respectively. The intensity of these two bands increases with increasing calcination temperature due to increasing the crystallinity. The formation of crystalline SiO_2 generates a substantial rise in intensity with a considerable shift of the bands when the calcination temperature is increased to 1000 °C. Small band corresponding to stretching vibration of Si–O bonds with one NBO, i.e. (Si–O–NBO) per SiO_4 terahedron (Q^3 groups) is detected at 900–975 cm^{-1} for the samples calcined at 600 and 800 °C. The absence of this band (Si–O–NBO) in the samples calcined at 1000 °C reflects a considerable increase in the local symmetry of the silicate network. Also, the lower field strength and electronegativity of Ca ions compared to Zn ions is responsible for the complete crystallization of the parent glass into calcium silicate ceramic as discussed before Eniu et al. [15]. The strong band centered at 1050 cm^{-1} is also attributed to the Si–O–Ca bond's stretching vibrational mode. This band indicates that Ca is inserted into the silicate-glass system owing to the existence of alkaline medium (as mentioned in experiments) but if this was in acidic medium, it would give heterogeneous Ca spreading. It should be noticed that the sharpness that occurs in bands located in the range 1250–800 cm^{-1} after calcination

at 1000 °C indicates the increasing of polymerization and organization for calcium silicate glasses. Therefore, crystallization is successfully carried out and calcium silicate ceramic is formed. New small bands at 630 and 700 cm^{-1} are developed after calcination at 1000 °C,these bands are indicating the formation of crystalline calcium-silicate phase. It has been recognized that the band of Zn–O bond is detectable in the range of 400–450 cm^{-1}, so in the current spectra, this band is confused with the broad band of Si–O-Si appeared at 450 cm^{-1}. It is expected that the band of Zn–O is more detectable for the sample Zn5 than Zn2 which contains lower amount of ZnO. With increasing the temperature, the bands in the range between 800 and 1250 cm^{-1} become sharper with the formation of Zn–O-Si and Ca-O-Si bonds in the produced materials and consequently the polymerization and crystallization are increased. It is worth noticing that the IR results obtained are equivalent to those acquired by XRD.

TEM-SAED was employed to examine the particle size and morphology as well as diffraction pattern of all prepared samples calcined at different temperatures as shown in Figs. 3 and 4. By careful analysis of TEM images (Figs. 3a and 4a) obtained for the material calcined at 600 °C, it is easy to observe that the particles have a high degree of agglomeration, they are very fine and still nearly to gel structure like the as-synthesized form. The reason behind this agglomeration is the extreme reactivity of fine and

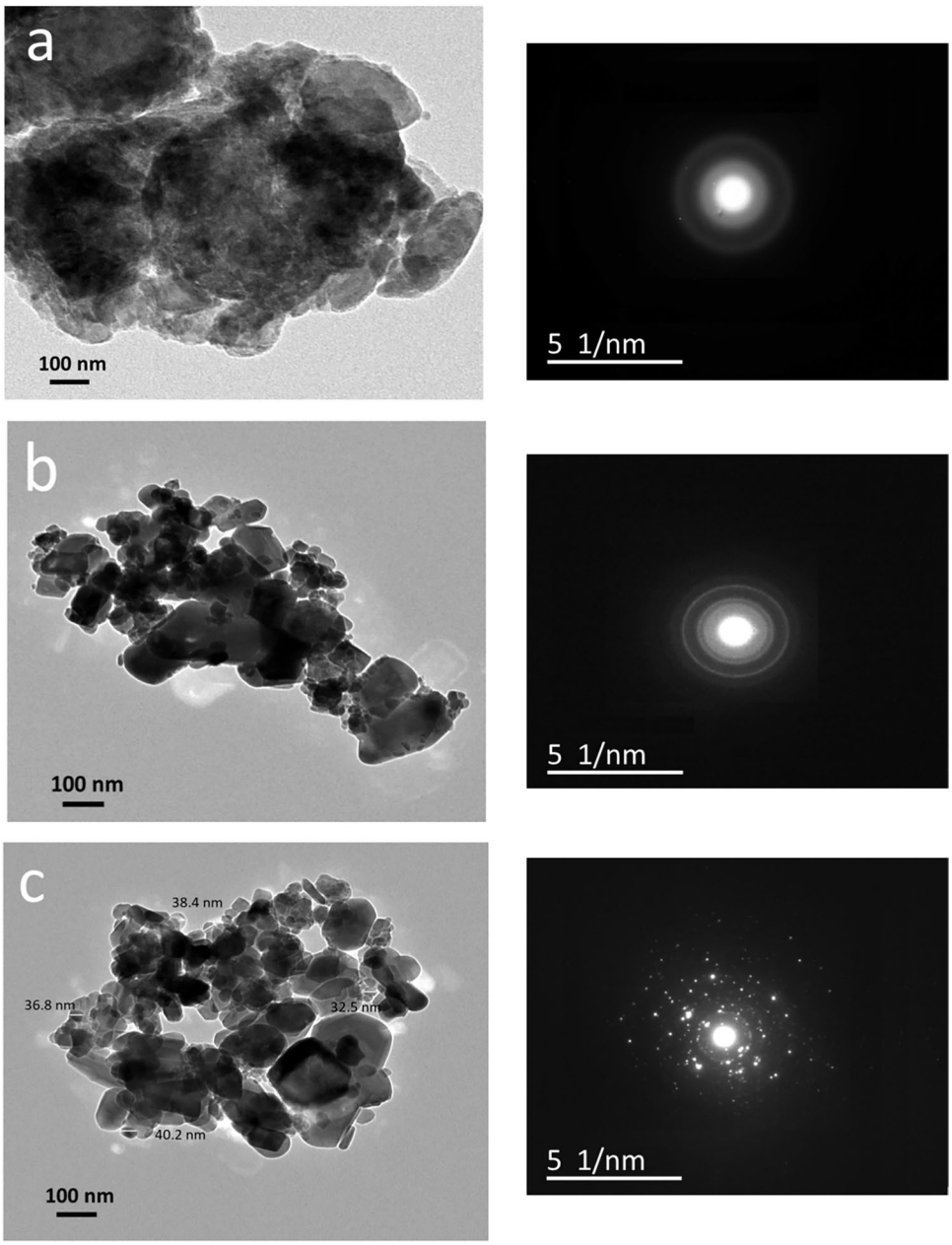

Fig. 3 TEM images and SAED patterns of Zn2 sample fired at (a) 600, (b) 800 and (c) 1000 °C

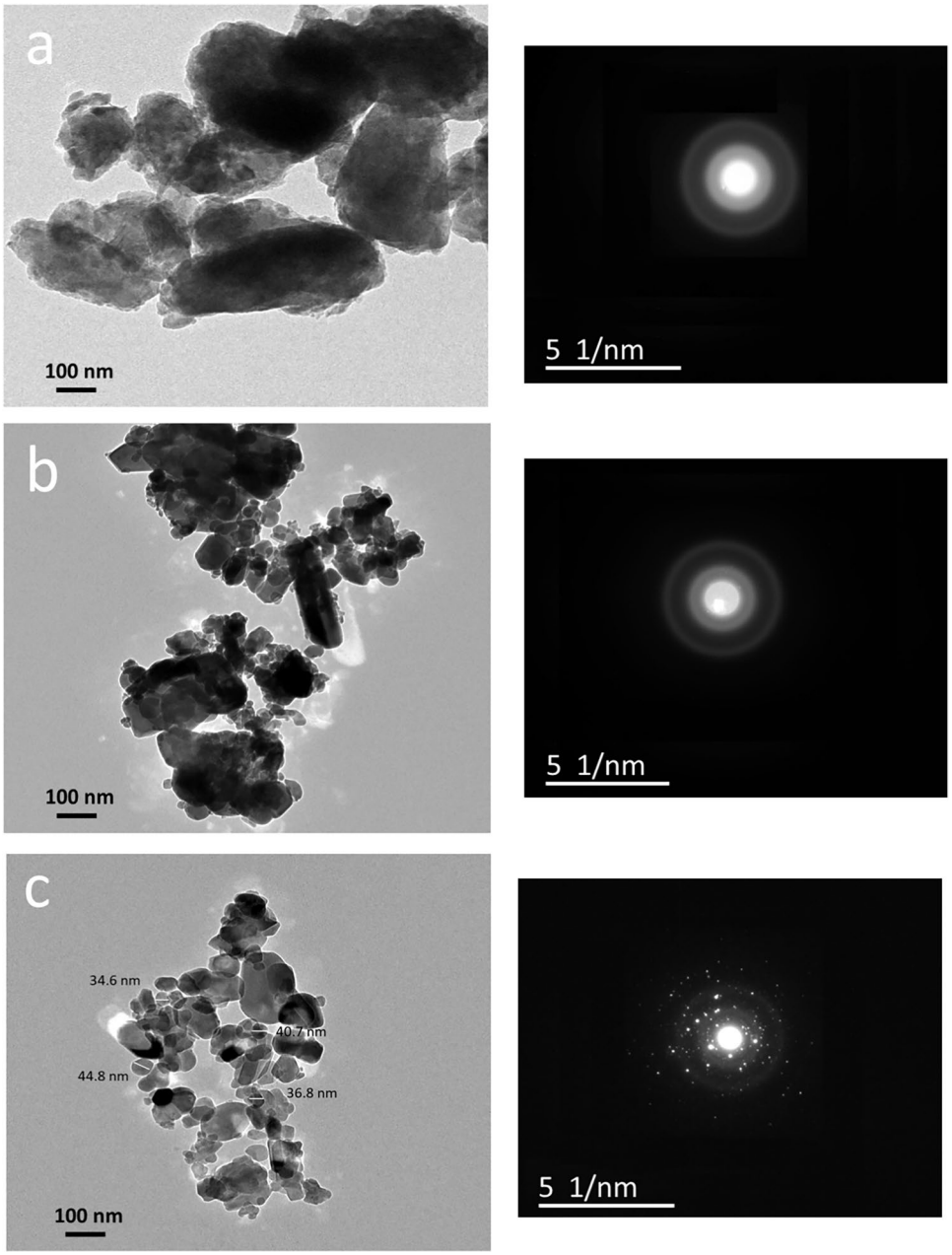

Fig. 4 TEM images and SAED patterns of Zn5 sample fired at (a) 600, (b) 800 and (c) 1000 °C

amorphous particles so they haven't defined morphology but they are still in gel structure. However, the gradual increase in calcination temperature into 800 and 1000 °C is responsible for considerable reduction in this undesirable agglomeration and for the emergence of the specific shape of particles. Well-defined edged and spherical particles are formed after increasing the calcination temperature into 800 and 1000 °C due to increasing the crystallinity. This is confirmed by the results of SAED; it can be seen that the samples calcined at 600 and 800 °C have an amorphous structure with no indication of crystal planes. On the opposite side, samples calcined at 1000 °C show polycrystalline diffraction rings belonging to CS, SiO_2 and ZnO, which may be recognized using the JCPDS card no.: 84–0655, 86–1629 and **89–5899**, respectively. After calcination at 1000 °C, the particles are still in the nanoscale range with an average size of 39 and 37 nm for Zn2 and Zn5 samples, respectively.

3.2 Properties of Sintered Ceramics

3.2.1 Physical Properties

It has been documented that the porous structure of biomaterials has a significant influence on their bioactivity since it improves the growing of apatite layer, similar to natural bone, on their surfaces and supports the path of

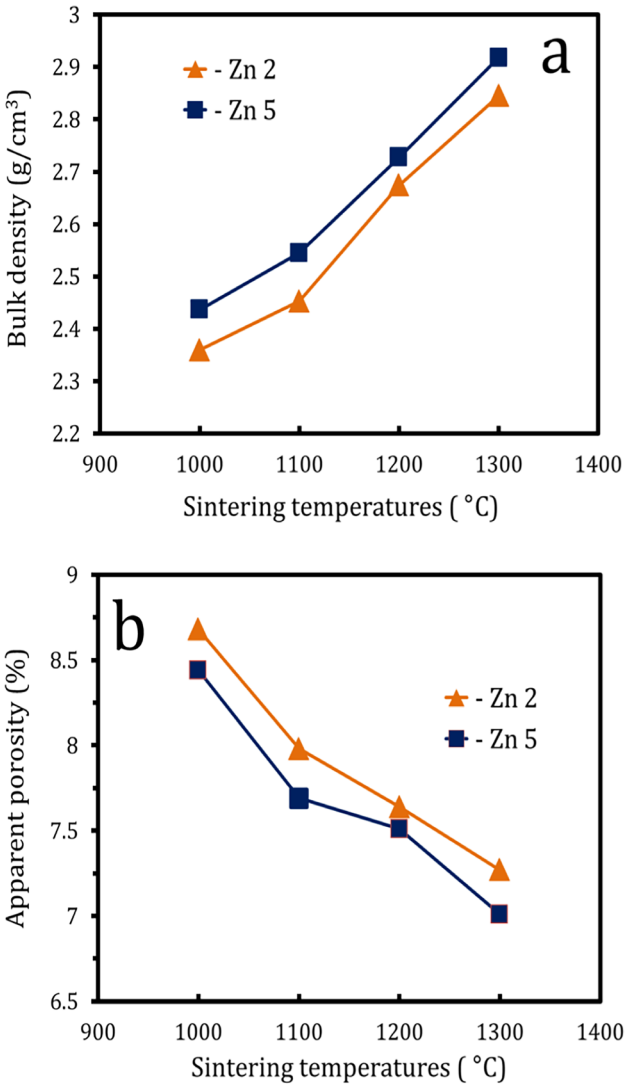

Fig. 5 Bulk density (a) and apparent porosity (b) of ceramics sintered at different firing temperatures

physiological fluids to bone center [14, 49]. Thus, the apparent porosity and bulk density of bio-materials are important parameters and should be assessed. The bulk-density and apparent-porosity of CaO–SiO–ZnO ceramics sintered at 1000°, 1100°, 1200°, and 1300 °C, are depicted in Fig. 5. The substitution of Ca by Zn results in a substantial rise in density values and decrease in apparent porosity. Two considerations can be presented to interpret this result. One of these consideration is the substitution of lighter CaO (density = 3.34 g/cm^3 and atomic mass = 56.07) with heavier ZnO (density = 5.61 g/cm^3 and atomic mass = 81.39) resulting in a noticeable rise in bulk density values. Secondly, the addition of zinc oxide leads to increase the diffusion of grains and increasing the densification though the formation of solid solution and/or intermediate phases in the CaO-ZnO-SiO_2 system. This interpretation is closely supported by those described in Ref. [15, 51]. It also indicated that the increase of sintering temperature has a significant impact on increasing the densification of sintered samples and closing pores. This is due to the diffusion of grains which promotes densification and grain growth [52] through the creation of necks and closed-off pores. This increases the bulk density and decreases the apparent porosity with increasing the sintering temperature [23, 46]). It should be emphasized that while porosity increases the biological performance of biomaterials, it has a negative influence on their mechanical characteristics,therefore striking a balance between apparent porosity and mechanical properties of biomaterials is critical issue [26].

3.2.2 Microstructure and Surface Roughness of Sintered Bodies

It is well known that the biological activity of materials is profoundly influenced by their microstructure, surface roughness and morphological properties [21]. Figures 6 and 7 show SEM images of calcium silicate ceramics that contains 2 and 5% ZnO sintered 1100 and 1300 °C, respectively. For the samples sintered at 1100 °C, interesting microstructures are obtained. Most of grains are hollow and some of them are compacted flat grains,the grain sizes are ranged between 1-5 µm. The formation of like-hollow grains is probably due to recrystallization and beginning of building flat edged grains as appeared in the microstructure of samples sintered at 1300 °C (Fig. 7). Also, some liquid phases are appeared around the grains. Moreover, both microstructures are permeable; the pore sizes and pore numbers are larger in the sample that contains 2% ZnO with the formation of small microcraks. Generally, these microstructures are relatively homogenous in grain sizes and shapes (Fig. 6). The creation of porous microstructure suggests that this temperature is insufficient to produce complete dense materials although it might be beneficial in some case for biomedical applications. For the samples sintered at 1300 °C (Fig. 7), the microstructures are relatively changed. Most of grains become flat and edged with very little hollow grains still unchanged. The microstructures are homogenous and compacted with relatively grain growth. The grains sizes are ranged between 5–10 µm. A few pores are appeared in the sample that contains 2% ZnO. The doped zinc oxide is appeared as white spots in the gray grains of calcium silicate ceramics; its amount is higher in the microstructure of the sample that contains 5% ZnO (Fig. 7b). Furthermore, some liquid phase thin films are detected on the grain boundaries. Also, some micro cracks are appeared in the microstructures.

Since the surface mapping of biomaterials is important for better understanding of how biomaterials interact with biological tissues which leads to osseointegration, thus this work is concerned with studying the surface roughness

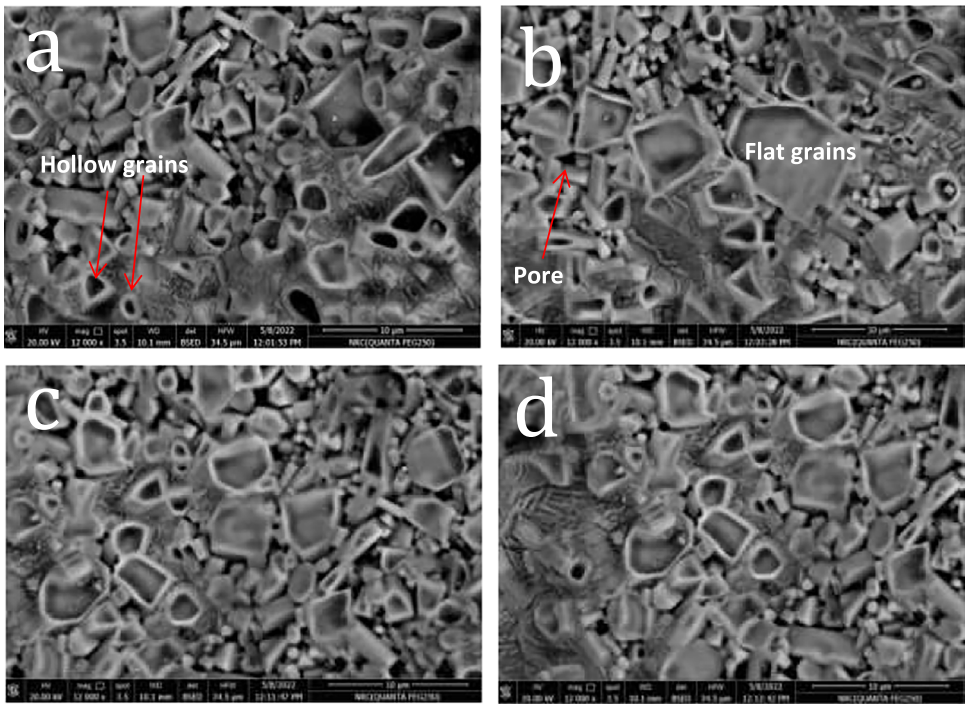

Fig. 6 SEM Images of Zn2 (different magnifications; a&b) and Zn5 (different magnifications; c&d) sintered at 1100 °C

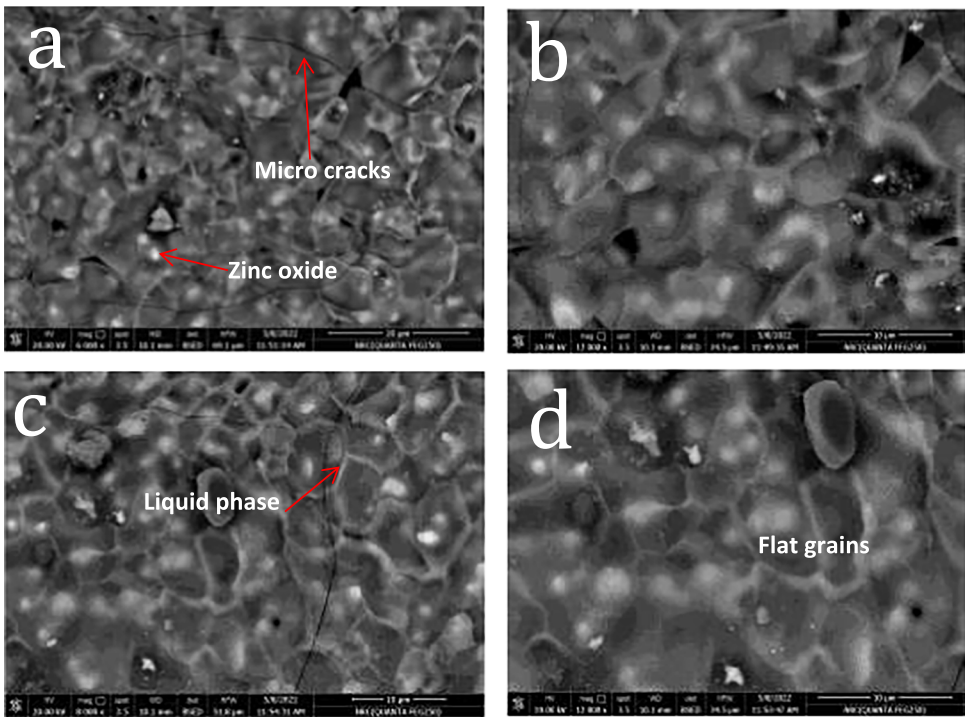

Fig. 7 SEM Images of Zn2 (different magnifications; a&b) and Zn5 (different magnifications; c&d) sintered at 1300 °C

of sintered specimens [39]. Figures 8 and 9 depict the surface roughness micrographs of calcium silicate ceramics that contains 2 and 5% ZnO sintered 1100 and 1300 °C, respectively. On the other hand, Table 2 illustrates the extracted parameters of surface roughness for the same samples. It can be seen form Figs. 8 and 9 and Table 2 that the roughness of the samples sintered at 1100 °C is higher than that sintered at 1300 °C. Also, a relatively similar roughness is obtained for the samples that contain 2 and 5% ZnO. The higher roughness of the samples sintered at 1100 °C is due to the higher porosity and formation of hollow grains after sintering at this temperature. As stated in Refs. [27, 39], the binding of osteoblast increases with increasing surface roughness. The increasing of surface

Table 1 Batch compositions of the prepared Zn-containing calcium silicates

Sample code	Calcination temperature (°C)	Chemical composition (mol.%)		
		Si	Ca	Zn
Zn2	600	85	13	2
	800			
	1000			
Zn5	600	85	10	5
	800			
	1000			

roughness leads to increasing the specific surface area and consequently accelerates the chemical reactions responsible for cell binding. The achieved surface roughness values are within the anticipated range for cell proliferation [38].

3.2.3 Mechanical Properties of Sintered Ceramics

It has been established that the mechanical properties of biomaterials effect seriously on their therapeutic applications. These characteristics depend mainly on the sintering temperature, type of material and additives as well as the physical properties of sintered materials that might enhance or deteriorate the mechanical properties of biomaterials which consequently reflect on the biological properties [45, 57]. In this context, micro-hardness (Hv) and fracture-toughness (K_{IC}) of the prepared ceramics (Zn2 and Zn5) sintered at different firing temperatures are shown in Fig. 10, while their compressive-strength is presented in Fig. 11. On the other hand, longitudinal- and shear-velocities are displayed in Fig. 12, while the Young's-modulus (E), longitudinal-modulus (L), bulk-modulus (K), shear-modulus (G) and

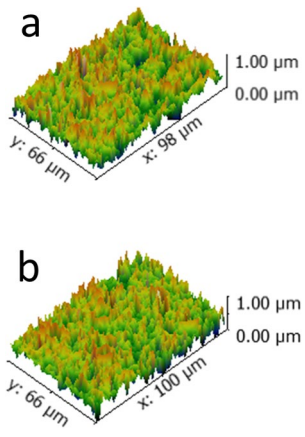

Fig. 8 Surface roughness of (a) Zn2 and (b) Zn5 samples sintered at 1100 °C

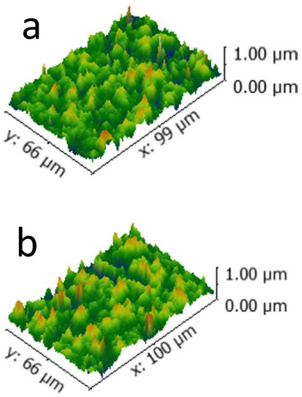

Fig. 9 Surface roughness of (a) Zn2 and (b) Zn5 samples sintered at 1300 °C

Poisson's-ratio (ν) of both bioceramics (Zn2 and Zn5) fired at various temperatures are and represented in Fig. 13. The obtained results indicate that the increase in ZnO content from 2 to 5 mol.% and the increase of sintering temperature from 1000 to 1300 °C are responsible for improving the fracture toughness of prepared sintered bioceramics (Fig. 10). This finding gives these materials great significance because the enhancement of fracture toughness is responsible for the long-term clinical success of biomaterial after implantation in the human body. However, the increase in Zn content leads to a slight reduction of other mechanical properties (hardness, compressive strength, elastic moduli and Poisson ratio),while the increasing the sintering temperature up to 1300 °C leads to improving the mechanical properties (Figs. 10–13). It is important to obtain biomaterials having comparable mechanical properties with those of human bone; otherwise the surrounding bone will suffer from the stress-shielded effect that severely weakens the bone. Despite the importance of matching the mechanical properties of biomaterials with those of living bone as mentioned before, increasing microhardness of a material reflects its

Table 2 Roughness parameters of biomaterials sintered at 1100 and 1300 °C

Parameters	1100 °C		1300 °C	
	Zn2	Zn5	Zn2	Zn5
Ra (nm)	41.5	42.1	31.6	32.2
Rq (nm)	53.5	57.0	40	41.8
Rt (nm)	434.7	532.8	311.9	398.6
Rv (nm)	224.0	251.0	144.7	221.9
Rp (nm)	210.7	281.8	167.1	176.8
Rpm (nm)	16.12	170.9	117.9	148.8

Ra: Roughness average

Rq: Root mean square roughness

Rt: Maximum height of the roughness

Rv: Maximum roughness valley depth

Rp: Maximum roughness peak height

Rpm: Average maximum roughness peak height

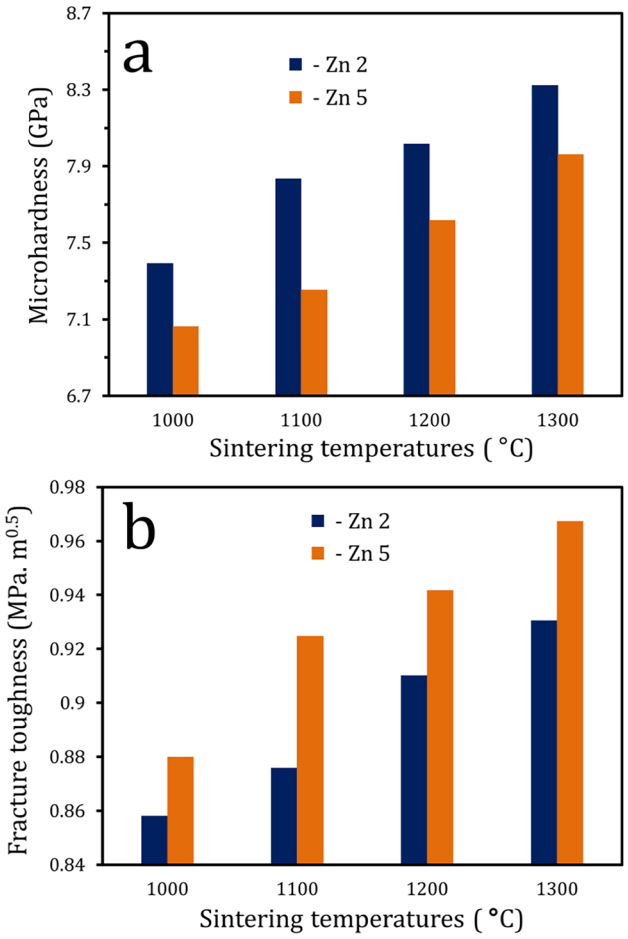

Fig. 10 Microhardness (a) and fracture toughness (b) of the samples sintered at different temperatures

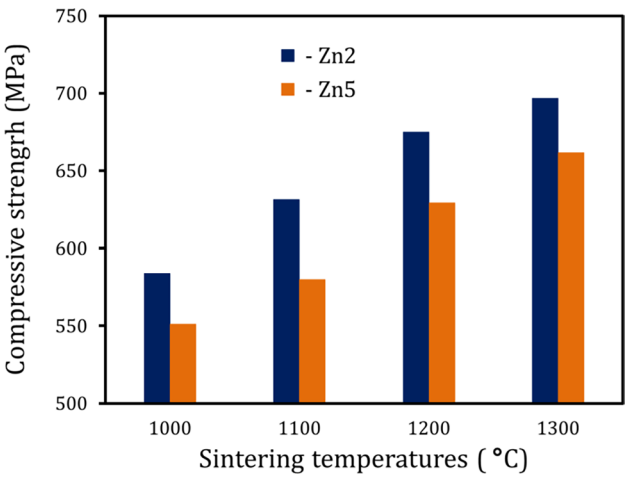

Fig. 11 Compressive strength of samples sintered at 1000, 1100, 1200 and 1300 °C

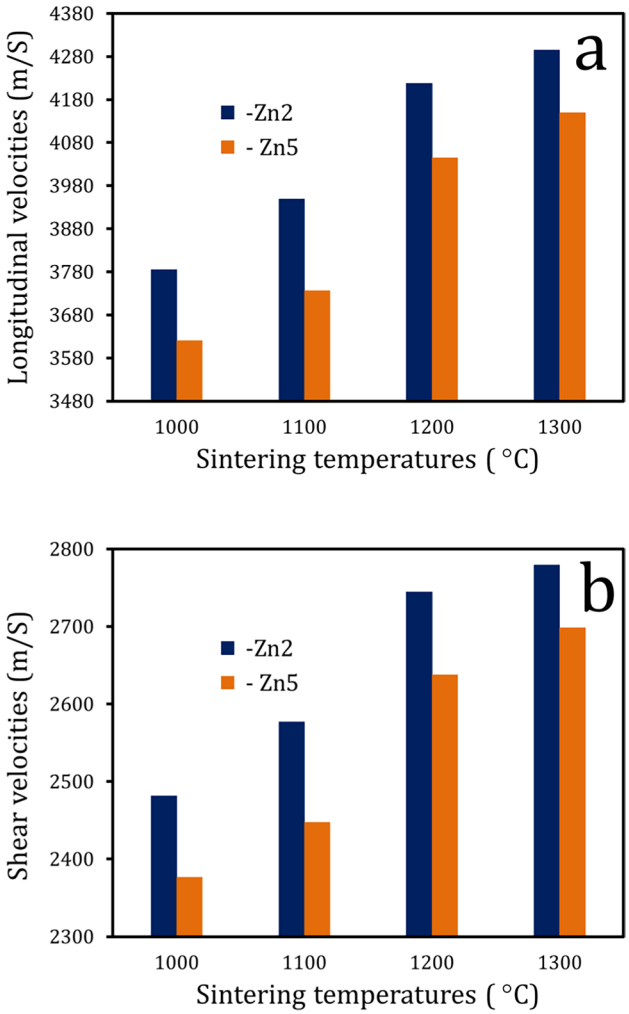

Fig. 12 Longitudinal (a) and shear (b) velocities of the samples sintered at different temperatures

higher wear resistance. This topic is extremely important to ensure the protection of these implants from the friction as a result of body weight and external loads. In other words, the identification of whether the suitable mechanical properties are high or matching those of bones is strongly based on whether these materials will be used for load-bearing or non-load-bearing sites applications.

Although the increasing of ZnO leads to slight decrease in porosity which is known to have positive effect on the hardness and compressive strength of materials, slight reduction in hardness and compressive strength is obtained. This is owing to the lower hardness value of sintered ZnO (1.5–1.83 GPa) as compared to that of silicate phases (6–8.5 GPa) [42, 48]). Increasing the sintering temperature up to 1300 °C, leads to increasing the grain-grain interaction with closing the pores which consequently enhances the hardness and compressive strength of the prepared materials. Figure 13 shows the values of elastic moduli of prepared bioceramics

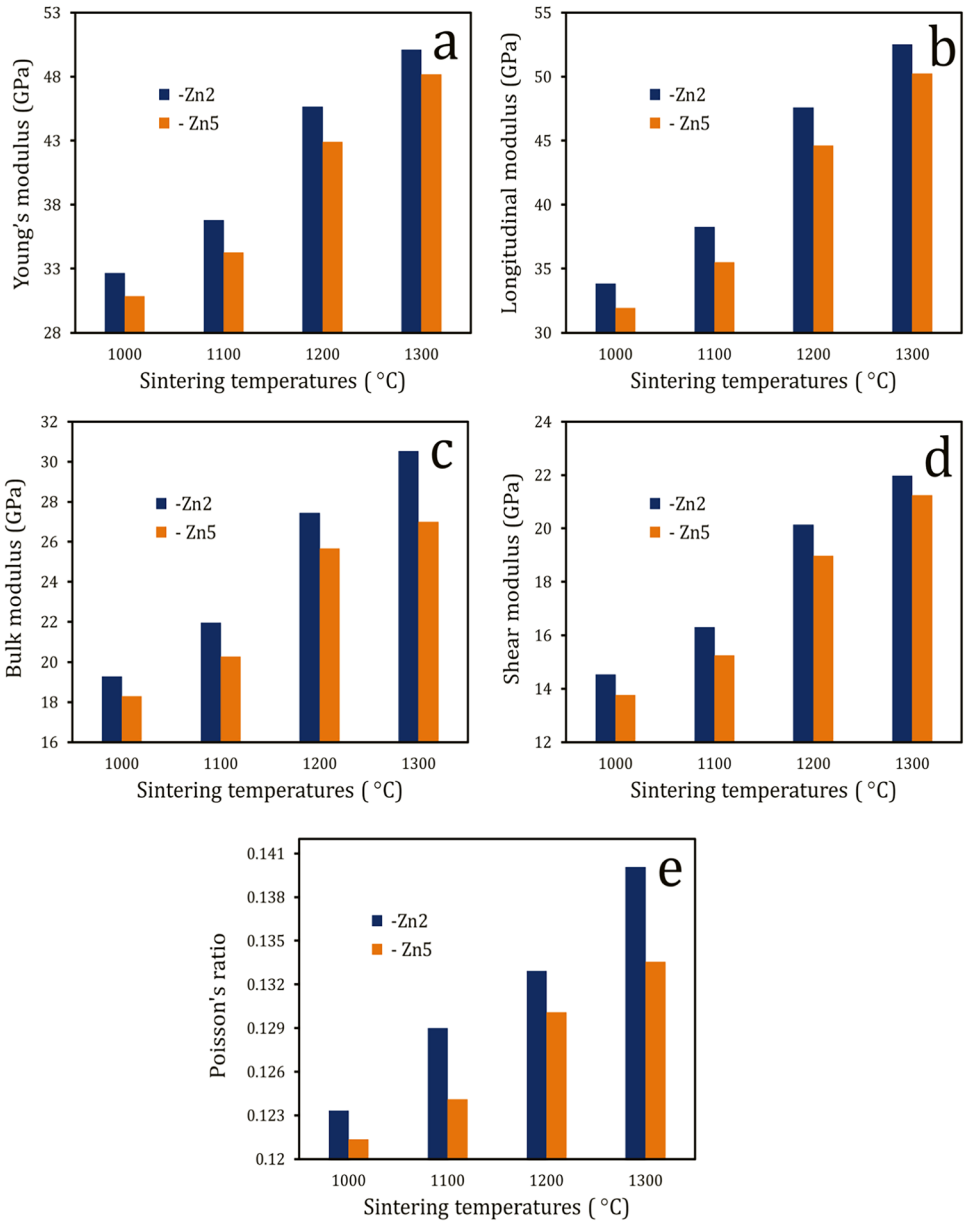

Fig. 13 Elastic moduli, i.e. a) Young's, b) longitudinal, c) bulk and d) shear modulus and e) Poisson's ratio, of the samples sintered at different temperatures

sintered at different temperatures. The same behavior is also indicated,the elastic moduli exhibit slight decrease after increasing ZnO content while they are increased after increasing the sintering temperature. The decrease in elastic-moduli with increasing the ZnO content is due to the lower elastic-moduli of ZnO as compared to that of silicate phases. The increase in elastic moduli with increasing of the sintering temperature is owing to the decrease in porosity and densification of sintered bioceramics. The bioceramics which have higher elastic moduli are not recommended for biomedical applications since the higher moduli values result in shielding stress due to the mismatching with those of human bone which causes some problem at the interface between the implant and the human bone [33]. However, osseointegration capability of CaO-ZnO-SiO_2 generates a strong bond at its interface with bone and reduces the probability for fracturing and delamination. For inhibition the bone absorption afterward implantation, lower elastic moduli is needed for biomaterials.

3.2.4 Electrical Characteristics of Sintered Ceramics

It has been recognized that the promotion of bone growth is seriously improved by biomaterials that have good

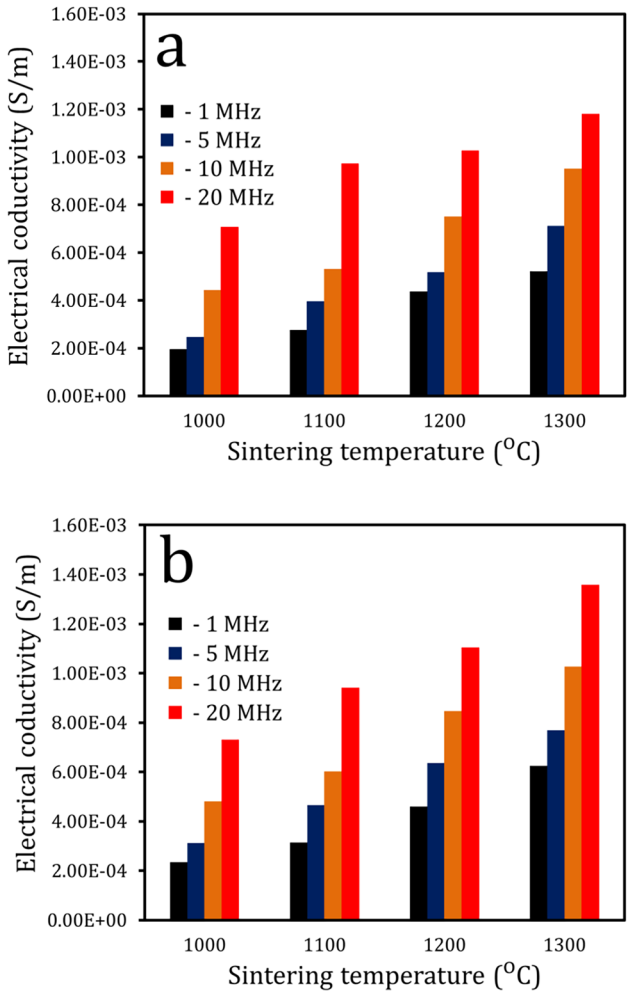

Fig. 14 Electrical conductivity at 1, 5, 10 and 20 MHz for a) Zn2 and b) Zn5 samples sintered at different temperatures

electrical properties. So it is important to study the electrical-conductivity, dielectric-constant and dielectric-loss at different frequencies, i.e. 1, 5, 10 and 20 MHz for prepared materials sintered at different temperatures as shown in Figs. 14–16. It can be seen from Fig. 14 that the AC conductivity increases not only with increasing Zn content but also with increasing the sintering temperature and applied frequency. This observation is consistent with the fact that electrical conductivity is a property that is influenced by many factors such as chemical composition, microstructure and porosity of sintered materials, as well as applied frequencies [35]. Based on this idea, the frequency change from 1 to 20 MHz, the replacement of Ca by Zn (up to 5 mol%) and the increase in sintering temperature up to 1300 °C are the main factors affecting the electrical conductivity of the investigated materials. This can be explained as follow: (i) considering that Zn has better electrical conductivity than Ca, (ii) the increasing of frequency up to 20 MHz facilitates the movement of charge carriers to move freely and thus increases the conduction mechanism of these samples [17] and (iii) obtaining dense microstructure with lower porosity after sintering at 1300 °C is the critical point to reach the best electrical conductivity. The reason for the positive effect of sintering temperature on the electrical conductivity is that the significant drop in porosity facilitates the electron transport. Since the pores in sintered samples are nonconductive, free electrons collide with a smaller number of pores on their path, so the electrical resistivity is decreased [47]. The results obtained are matched with those described elsewhere [36].

The following equation [13] is used to illustrate the material's complex dielectric constant:

$$\varepsilon = \varepsilon' + j\varepsilon'' \tag{1}$$

Since: ε′ refers to real component of dielectric-constant which measures the stored energy from the applied electric-field and defines the alignment of dipoles in the material. In contrast, ε″ indicates the energy wasted in the dielectric and refers to imaginary component of dielectric-constant, i.e. dielectric-loss.

In ceramic materials, the charge carriers cannot move freely unless an alternating field is applied to cause polarization [25]. As the frequency rises, the charge carriers transfer across the dielectric and become trapped against a defect site, where they generate an opposing charge, slowing the migration of charge carriers and lowering the value of the dielectric constant [18]. Therefore, as indicated in Fig. 15, the dielectric constant decreases with increasing frequency. It is also indicated from Fig. 15 that the dielectric constant decreases with increasing ZnO content and increases with increasing sintering temperature. The reduction of dielectric constant with increasing the zinc oxide amount can be explain by the fact that ZnO has good dielectric properties, low dielectric loss, and high electrical resistivity than calcium silicate phases. The increasing of dielectric constant with increasing the sintering temperature is owing to reduction of porosity with increasing the grain boundary connection and structural properties improvement. On the other side, the frequency dependence of dielectric loss is closely related to conductance, ion relaxation, deformation, and vibration. Conductance and ion relaxation are the major sources of dielectric loss at low frequencies. While, the other two factors become more prominent at higher frequencies. As seen in Fig. 16,

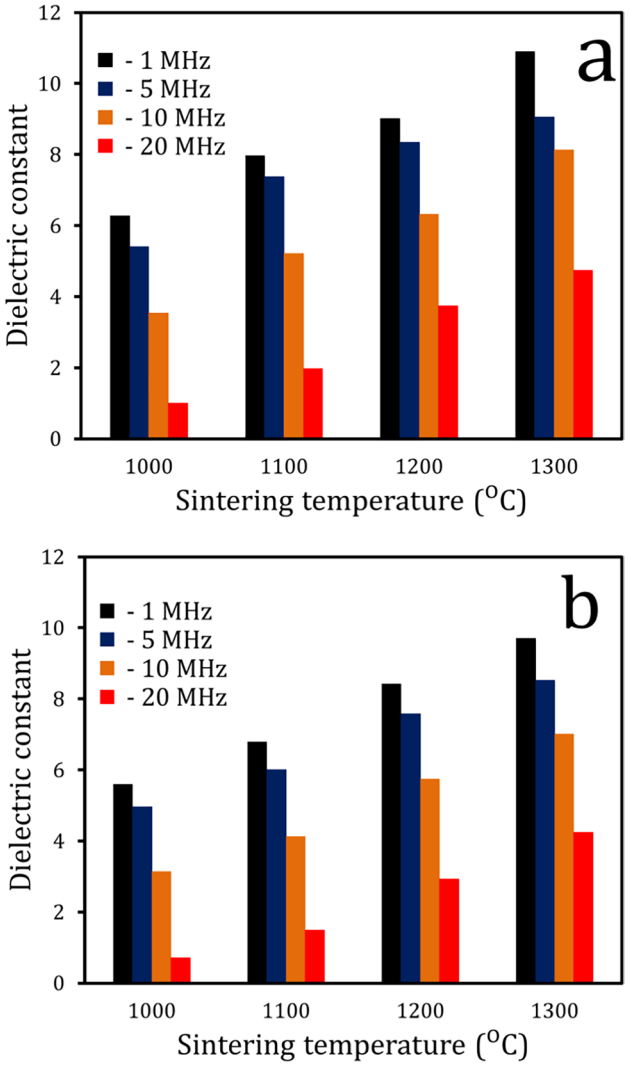

Fig. 15 Dielectric constant at 1, 5, 10 and 20 MHz for a) Zn2 and b) Zn5 samples sintered at different temperatures

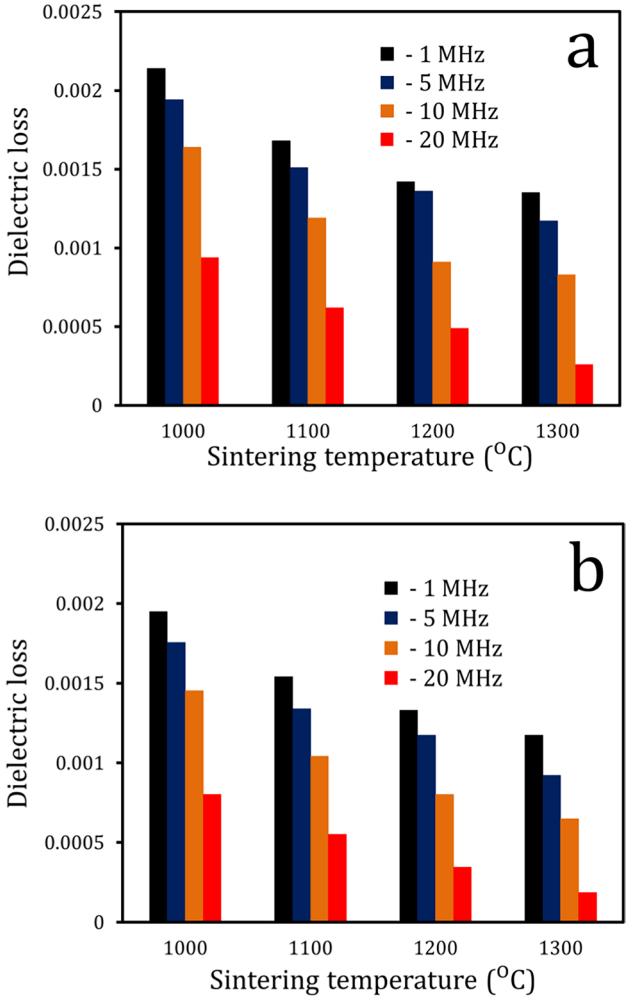

Fig. 16 Dielectric loss at 1, 5, 10 and 20 MHz for a) Zn2 and b) Zn5 samples sintered at different temperatures

the dielectric loss decreases with increasing frequency, sintering temperature and ZnO content. This is due to the aforementioned reasons.

4 Conclusion

In this work, nano amorphous and crystalline calcium silicates doped with various mole percentages of ZnO were successfully prepared by sol–gel method after calcination at different temperatures, i.e. 600, 800 and 1000 °C. The materials retained amorphous after calcination up to 800 °C, but they changed into crystalline after calcination at 1000 °C. When those powders sintered at different temperatures exhibited good physical, mechanical and electrical properties. With increasing both sintering temperature and ZnO concentration, the bulk density, fracture toughness and electrical conductivity were increased. On the other side, the hardness, compressive strength, elastic moduli and Poisson ration were increased with increasing sintering temperature and decreased with increasing zinc content.

Author Contributions Rasha A. Youness, Mahmoud F. Zawrah, Mohammed A. Taha contributed to the study conception and design. Material preparation, data collection and analysis were performed by Rasha A. Youness and Mohammed A. Taha. The first draft of the manuscript was written by Rasha A. Youness, Mahmoud F. Zawrah, Mohammed A. Taha and all authors commented on previous

versions of the manuscript. All authors read and approved the final manuscript.

Funding The authors declare that no funds, grants, or other support were received during the preparation of this manuscript.

Data Availability All date was presented in the article.

Declarations

Competing interests The authors declare no competing interests.

Ethics approval Not applicable.

Competing of interest The authors have no relevant financial or non-financial interests to disclose.

Consent to participate Not applicable.

Consent for publication Not applicable.

References

1. Abdel Aal A, Hammad TR, Zawrah MF, Battisha IK, Abou Hammad AB (2014) FTIR Study of nanostructure perovskite $BaTiO_3$ doped with both Fe^{3+} and Ni^{2+} ions prepared by sol-gel technique. Acta Phys Pol A 126(6):1318–1321
2. Aina V, Malavasi G, Pla AF, Munaron L, Morterra C (2009) Zinc-containing bioactive glasses: surface reactivity and behavior towards endothelial cells. Acta Biomater 5:1211–1222
3. Alatawi AS, Alturki AM, Soliman GM, Abulyazied DE, Taha MA, Youness RA (2021) Improved toughness, electrical conductivity and optical properties of bioactive borosilicate glasses for orthopedic applications. Appl Phys A 127(971):1–13
4. Alawad OA, Alhozaimy A, Jaafar MS, Aziz FNA, Al-Negheimish A (2015) Effect of autoclave curing on the microstructure of blended cement mixture incorporating ground dune sand and ground granulated blast furnace slag. Int J Concr Structures Mater 9(3):381–390
5. Arcos D, Vallet-Regi M (2010) Sol-gel silica-based biomaterials and bone tissue regeneration. Acta Biomater 6(8):2874–2888
6. Atkinsona I, Anghela EM, Predoana L, Mocioiu OC, Jecub L, Raut I, Munteanu C, Culita D, Zaharescu M (2016) Influence of ZnO addition on the structural, in vitro behavior and antimicrobial activity of sol–gel derived $CaO–P_2O_5–SiO_2$ bioactive glasses. Ceram Int 42:3033–3045
7. Baciu D, Simitzis J (2008) Synthesis and characterization of a calcium silicate bioactive glass. J Optoelectron Adv Mater 9(11):3320–3324
8. Bahir MM, Khairnar RS, Mahabole MP (2020) Electrical properties of newly calcified tissues on the surface of silver ion administrated hydroxyapatite scaffolds. J Biomater Nanobiotechnol 11:83–100
9. Balasubramanian P, Strobel LA, Kneser U, Boccaccini AR (2019) Zinc-containing bioactive glasses for bone regeneration, dental and orthopedic applications. Biomed Glasses 1:51–69
10. Brescó MS, Harris LG, Thompson K, Stanic B, Morgenstern M, O'Mahony L, Richards RG, Moriarty TF (2017) Pathogenic mechanisms and host interactions in Staphylococcus epidermidis device-related infection. Front Microbiol 8:1–24
11. Deshmukh K, Kovářík T, Křenek T, Docheva D, Stich T, Pola J (2020) Recent advances and future perspectives of sol–gel derived porous bioactive glasses: a review. RSC Adv 10:33782–33834
12. Dhmees AS, Rashad AM, Eliwa AA, Zawrah MF (2019) Preparation and characterization of nano $SiO_2@CeO_2$ extracted from blast furnace slag and uranium extraction waste for wastewater treatment, Ceramics International. Ceram Int 45:7309–7317
13. Elbashar YH, Badr AM, Elshaikh HA, Mostafa AG, Ibrahim AM (2016) Dielectric and optical properties of CuO containing sodium zinc phosphate glasses. Process Appl Ceram 10(4):277–286
14. Encinas-Romero MA, Peralta-Haley J, Valenzuela-Garcia JL, Castillon-Barrza FF (2013) Synthesis and microstructural characterization of hydroxyapatite wollastonite biocomposites, produced by an alternative sol-gel route. Biomater Nanotechnol 4:327–333
15. Eniu D, Gruian C, Vanea E, Patcas L, Simon V (2015) FTIR and EPR spectroscopic investigation of calcium-silicate glasses with iron and dysprosium. J Mol Struct 1084:23–27
16. Enrique Rocha-Rangel (2011) Fracture toughness determinations by means of indentation fracture, 22–38. https://doi.org/10.5772/18127
17. EzzEldin FM, Alaily NA (1998) Electrical conductivity of some alkali silicate glasses. Mater Chem Phys 52:175–179
18. Fares S (2011) Frequency dependence of the electrical conductivity and dielectric constants of polycarbonate (Makrofol-E) film under the effects of γ-radiation. Nat Sci 3(12):1034–1039
19. Fehr KT, Huber AL (2001) Stability and phase relations of $Ca[ZnSi_3]O_8$, a new phase with feldspar structure in the system $CaO-ZnO-SiO_2$. Am Mineral 86:21–28
20. Frassinetti S, Bronzetti GL, Caltavuturo L, Cini M, Croce CD (2006) The role of zinc in life: a review. J Environ Pathol Toxicol Oncol 25(3):597–610
21. Glasser FP, Macphee DE, Lachowski EE (2011) Solubility modeling of cements: implications for radioactive waste immobilisation. MRS Proc 84:331–341
22. Greenberg SA, Chang TN (1965) Investigation of the colloidal hydrated calcium silicates. II. Solubility relationships in the calcium oxide-silica-water system at 25°C. J Phys Chem. 69(1):182–188
23. Hamzawy EM, El-Kheshen AA, Zawrah MF (2005) Densification and properties of glass/cordierite composites. Ceram Int 31(3):383–389
24. Hench LL, Splinter RJ, Allen WC, Greenlee TK (1971) Bonding mechanisms at the interface of ceramic prosthetic materials. J Biomed Mater Res 5:117–141
25. Ibrahim S, Darwish H, Gomaa MM (2012) Electrical and physicochemical properties of some Ag_2O-containing lithia iron silica phosphate glasses. J Mater Sci Mater Electron 23:1131–1142
26. Jain D, Shivani BAA, Singh H, Daima HK, Singh M, Mohanty SR, Stephen BJ, Singh A (2020) Microbial fabrication of zinc oxide nanoparticles and evaluation of their antimicrobial and photocatalytic properties. Front Chem 81:1–11
27. Kamarajan BP, Thankappan S, Muthusamy A (2015) Relevance of surface asperities in scheming cellular attachment to minimize biomaterial associated infections. Trends Biomater Artif Organs 29(2):140–145
28. Kayani ZN, Iqbal M, Riaz S, Zia R, Naseem S (2015) Fabrication and properties of zinc oxide thin film prepared by sol-gel dip coating method. Mater Sci Poland 33(3):515–520
29. Kenway MH, El-Hadad AA, Soliman IE, Ereiba KMT (2016) Bioactivity and characterization study of synthetic zirconia-silicate sol-gel glass powder. Middle East J Appl Sci 6(2):329–340
30. Khalil EMA, Youness RA, Amer MS, Taha MA (2018) Mechanical properties, in vitro and in vivo bioactivity assessment of $Na_2O-CaO-P_2O_5-B_2O_3-SiO_2$ glass-ceramics. Ceram Int 44(7):7867–7876
31. Kołodziejczak-Radzimska A, Jesionowski T (2014) Zinc oxide—from synthesis to application: a review. Materials 7(4):2833–2881
32. Maeda H, Nakano Y, Kasuga T (2013) Preparation of $CaO-SiO_2$ glass-ceramic spheres by electrospraying combined with sol-gel method. J Nanomater 2013:1–5

33. Mehrali M, Shirazi FS, Metselaar HSC, Kadri NAB, Osman NAA (2013) Dental implants from functionally graded materials. J Biomed Mater Res Part A 101a:3046–3057
34. Mourino V, Cattalini JP, Boccaccini AR (2012) Metallic ions as therapeutic agents in tissue engineering scaffolds: an overview of their biological applications and strategies for new developments. J R Soc Interface 9:401–419
35. Moustafa EB, Taha MA (2020) Preparation of high strength graphene reinforced Cu based nanocomposites via mechanical alloying method: microstructural, mechanical and electrical properties. Appl Phys A 126(220):1–16
36. Moustafa EM, Taha MA (2021) Evaluation of the microstructure, thermal and mechanical properties of Cu/SiC nanocomposites fabricated by mechanical alloying. Int J Min Metall Mater 28(3):475–486
37. Owens GJ, Singh RK, Foroutan F, Alqaysi M, Han CM, Mahapatra C, Kim HW, Knowles JC (2016) Sol-gel based materials for biomedical applications. Prog Mater Sci 77:1–79
38. Rechendorff K, Hovgaard MB, Foss M et al (2006) Enhancement of protein adsorption induced by surface roughness. Langmuir 22:10885–10888
39. Rodrigues M, Da Cruz NC, Rocha JAF, Sá RCL, Bock EGP (2019) Surface roughness of biomaterials and process parameters of titanium dioxide gritblasting for productivity enhancement. TAS J 3(2):169–176
40. Sadek HEH, Khattab RM, Gaber AA, Zawrah MF (2014) Nano $Mg_{1-x}Ni_xAl_2O_4$ Spinel Pigments for Advanced Applications. Spectrochimica Acta: Mol Biomol Spectrosc 125(5):353–358
41. Serra J, Gonzalez P, Liste S, Chiussi S, Leon B, Perez-Amor M (2002) Influence of the non-bridging oxygen groups on the bioactivity of silicate glasses. J Mater Sci Mater Med 13:1221–1225
42. Shirazi FS, Mehrali M, Oshkour AA, Metselaar HSC, Kadri NA, Abu Osman NA (2014) Mechanical and physical properties of calcium silicate/alumina composite for biomedical engineering applications. J Mech Behav Biomed Mater 30:168–175
43. Speakman K (1968) The stability of tobermorite in the system $CaOSiO_2$-H_2O at elevated temperatures and pressures. Mineral Mag J Mineral Soc 36(284):1090–2103
44. Suri J, Shaw LL, Zawrah MF (2011) Synthesis of Carbon-Free Si_3N_4/SiC Nanopowders using Silica Fume. Ceram Int 37:3477–3487
45. Taha MA, Youness RA, Zawrah MF (2019) Review on nanocomposites fabricated by mechanical alloying. Int J Miner Metall Mater 26(9):1047–1058
46. Taha MA, Zawrah MF (2020) Fabrication of Al_2O_3-ZrO_2-Ni composites with improved toughness using nano powders prepared by mechanical alloying. Ceram Int 46:19519–19529
47. Taha Mohammed A, Youness RA, Zawrah MF (2020) Phase composition, sinterability and bioactivity of amorphous nano-CaO-SiO_2-CuO powder synthesized by sol-gel technique. Ceram Int 46:24462–24471
48. Tapatee KR (2015) Assessing hardness and fracture toughness in sintered zinc oxide ceramics through indentation technique. Mater Sci Eng, A 640:267–274
49. Wahsh MMS, Khattab RM, Zawrah MF (2013) Sintering and technological properties of alumina/zirconia/nano TiO_2 ceramic composites. Mater Res Bull 48(4):1411–1414
50. Wajdaa A, Goldmann WH, Detsch R, Boccaccini AR, Sitarz M (2019) Influence of zinc ions on structure, bioactivity, biocompatibility and antibacterial potential of melt-derived and gel-derived glasses from CaO-SiO_2 system. J Non-Cryst Solids 511:86–99
51. Wang Y, Zhu C, Parsons A, Rudd C, Ahmed I, Sharmin N (2019) Effects of ZnO addition on thermal properties, degradation and biocompatibility of $P_{45}Mg_{24}Ca_{16}Na_{(15-x)}Zn_x$. Biomed Glasses 5:53–66
52. Youness RA, Taha MA, El-Kheshen AA, Ibrahim M (2018) Influence of the addition of carbonated hydroxyapatite and selenium dioxide on mechanical properties and in vitro bioactivity of borosilicate inert glass. Ceram Int 44:20677–20685
53. Yue H, Wang X, Yang Z, Wei C (2017) Dynamic hydrothermal synthesis of super-low density xonotlite thermal insulation materials from industrial quartz powder. Key Eng Mater 14(2):215–228
54. Zawrah MF, Abo Mostafa H, Taha MA (2019) Effect of SiC content on microstructure, mechanical and electrical properties of Al-20Si-xSiC nanocomposites fabricated by mechanical alloying. Mater Res Express 6(12):125014
55. Zawrah MF, El-Gezary M (2007) Mechanical properties of SiC ceramics by ultrasonic nondestructive technique and its bioactivity. Mater Chem Phys 106:330–337
56. Zawrah MF, Schneider J, ZumGahr K-H (2002) Microstructure and Mechanical Characteristics of Laser-Alloyed Alumina Ceramics. J Material Sci Eng A 332(1–2):167–173
57. Zawrah MF, Shehata AB, Kishar EA, Yamani RN (2011) Synthesis, Hydration and Sintering of Calcium Aluminate Nanopowder for Biomedical Applications. C R Chim 14:611–618
58. Zhao R, Shi L, Gu L, Qin X, Song Z, Fan X, Zhao P, Li C, Zheng H, Li Z, Wang Q (2021) Evaluation of bioactive glass scaffolds incorporating SrO or ZnO for bone repair: in vitro bioactivity and antibacterial activity, J Appl Biomater Funct Mater 19
59. Zhu Y-J, Guo X-X, Sham T-K (2017) Calcium silicate-based drug delivery systems. Expet Opin Drug Deliv 14(2):215–228